Microwave photovoltage and photoresistance effects in ferromagnetic microstrips

N. Mecking,[1,2,*] Y. S. Gui,[1] and C.-M. Hu[†]
[1]*Department of Physics and Astronomy, University of Manitoba, Winnipeg, Canada R3T 2N2*
[2]*Institut für angewandte Physik und Zentrum für Mikrostrukturforschung, Universität Hamburg, Jungiusstraße 11, 20355 Hamburg, Germany*

(Received 23 August 2007; revised manuscript received 4 November 2007; published 27 December 2007)

We investigate the dc electric response induced by ferromagnetic resonance in ferromagnetic Permalloy ($Ni_{80}Fe_{20}$) microstrips. The resulting magnetization precession alters the angle of the magnetization with respect to both dc and rf current. Consequently the time averaged anisotropic magnetoresistance (AMR) changes (photoresistance). At the same time the time-dependent AMR oscillation rectifies a part of the rf current and induces a dc voltage (photovoltage). A phenomenological approach to magnetoresistance is used to describe the distinct characteristics of the photoresistance and photovoltage with a consistent formalism, which is found in excellent agreement with experiments performed on in-plane magnetized ferromagnetic microstrips. Application of the microwave photovoltage effect for rf magnetic field sensing is discussed.

DOI: 10.1103/PhysRevB.76.224430 PACS number(s): 76.50.+g, 75.30.Gw, 07.57.Kp

I. INTRODUCTION

The fact that macroscopic mutual actions exist between electricity and magnetism has been known for centuries as described in many textbooks of electromagnetism.[1] Now, this subject is transforming onto the microscopic level, as revealed in various spin-charge coupling effects studied in the new discipline of spintronics. Among them, striking phenomena are the dc charge transport effects induced by spin precession in ferromagnetic metals, which feature both academic interest and technical significance.[2,3] Experiments have been performed independently by a number of groups on devices with different configurations.[4–16] Most works were motivated by the study of spin torque,[17,18] which describes the impact of a spin-polarized charge current on the magnetic moment. In this context, Tulapurkar *et al.* made the first spin-torque diode,[4] and Sankey *et al.* detected the spin-torque-driven ferromagnetic resonance (FMR) electrically.[5] Both measured the vertical transport across nanostructured magnetic multilayers. Along a parallel path, a number of works[19–21] have been devoted to study the effect of spin pumping. One of the interesting predictions is that injection of a spin current from a moving magnetization into a normal metal induces a dc voltage across the interface. To detect such a dc effect induced by spin pumping,[20] experiments have been performed by measuring lateral transport in hybrid devices under rf excitation.[6–8]

From a quite different perspective, Gui *et al.* set out to explore the general impacts of the high frequency response on the dc transport in ferromagnetic metals,[9] based on the consideration that similar links in semiconductors have been extensively applied for electrical detection of both spin and charge excitations.[22] Gui *et al.* detected, subsequently, photoresistance induced by bolometric effect,[9] as well as photocurrent,[10] photovoltage,[11] and photoresistance[12] caused by the spin-rectification effect. A spin dynamo[10] was thereby realized for generating dc current via the spin precession, and the device was applied for a comprehensive electrical study of the characteristics of quantized spin excitations in microstructured ferromagnets.[11] The spin-rectification effect was independently investigated by both Costache *et al.*[13] and Yamaguchi *et al.*[14] and seems to be also responsible for the dc effects detected earlier by Oh *et al.*[15] A method for distinguishing the photoresistance induced by either spin precession or bolometric effect was recently established,[12] which is based on the nice work performed by Goennenwein *et al.*,[16] who determined the response time of the bolometric effect in ferromagnetic metals.

While most of these studies, understandably, tend to emphasize the different nature of dc effects investigated in different devices, it is perhaps more intriguing to ask the questions of whether the seemingly diverse but obviously related phenomena could be described by a unified phenomenological formalism and whether they might arise from a similar microscopic origin. From a historical perspective, these two questions reflect exactly the spirit of two classic papers[23,24] published by Juretscheke and Silsbee *et al.*, respectively, which have been often ignored but have shed light on the dc effects of spin dynamics in ferromagnets. In the approach developed by Juretscheke, photovoltage induced by FMR in ferromagnetic films was described based on a phenomenological depiction of magnetoresistive effects.[23] While in the microscopic model developed by Silsbee *et al.* based on the combination of Bloch and diffusion equations, a coherent picture was established for the spin transport across the interface between ferromagnets and normal conductors under rf excitation.[24]

The goal of this paper is to provide a consistent view for describing photocurrent, photovoltage, and photoresistance of ferromagnets based on a phenomenological approach to magnetoresistance. We compare the theoretical results with experiments performed on ferromagnetic microstrips in detail. The paper is organized in the following way: In Sec. II, a theoretical description of the photocurrent, photovoltage, and photoresistance in thin ferromagnetic films under FMR excitation is presented. Sections II A–II D establish the formalism for the microwave photovoltage (PV) and photoresistance (PR) based on the phenomenological approach to magnetoresistance. These arise from the nonlinear coupling of microwave spin excitations (resulting in magnetization **M** precession) with charge currents by means of the anisotropic

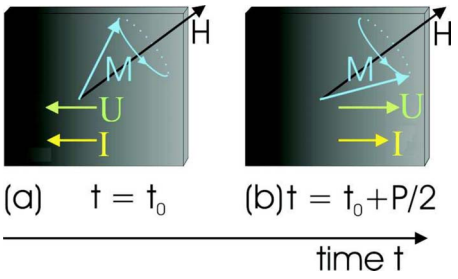

FIG. 1. (Color online) Mechanism of the AMR-induced microwave photovoltage: **M** precesses (period P) in phase with the rf current **I**. (a) **M** lying almost perpendicular to **I** results in low AMR. (b) **M** lying almost parallel to **I** results in high AMR. The time average voltage **U** becomes nonzero.

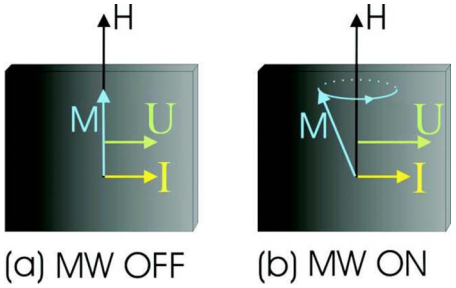

FIG. 2. (Color online) Mechanism of the AMR-induced photoresistance. (a) Without microwaves (MW) **M** lies perpendicular to the dc current **I** and the AMR is minimal (b) With microwaves **M** precesses and is not perpendicular to **I** anymore. Consequently the AMR increases (higher voltage drop **U**).

magnetoresistance (AMR). Section II E compares our model with the phenomenological approach developed by Juretscheke. Section II F provides a discussion concerning the microwave photovoltage and photoresistance based on other magnetoresistance effects [like anomalous Hall effect (AHE), giant magnetoresistance (GMR), and tunneling magnetoresistance (TMR)].

Experimental results on microwave photovoltage and photoresistance measured in ferromagnetic microstrips are presented in Secs. III and IV, respectively. We focus in particular on their characteristic different line shapes, which can be well explained by our model. In Sec. V conclusions and an outlook are given.

II. MICROWAVE PHOTOVOLTAGE AND PHOTORESISTANCE BASED ON PHENOMENOLOGICAL AMR

A. AMR coupling of spin and charge

The AMR coupling of spin and charge in ferromagnetic films results in microwave photovoltage and photoresistance. The photovoltage can be understood regarding Ohms law [current $I(t)$ and voltage $U(t)$]

$$U(t) = R(t) \cdot I(t). \tag{1}$$

We consider a time-dependent resistance $R(t)=R^0+R^1\cos(\omega t-\psi)$ which oscillates at the microwave frequency $\omega=2\pi f$ due to the AMR oscillation arising from magnetization precession. ψ is the oscillations phase shift with respect to the phase of the rf current $I(t)$. For the sake of generality ψ will be kept as a parameter in this work and will be discussed in detail in Sec. III C. $I(t)$ takes the form $I(t)=I_1\cos(\omega t)$ and is induced by the microwaves. It follows that $U(t)$ consists of time-dependent terms with the frequency ω, 2ω and a constant term (time independent) which corresponds to the time average voltage and is equal to the photovoltage: $U_{\mathrm{MW}}=\langle R^1 I_1\cos(\omega t-\psi)\cos(\omega t)\rangle=(R^1 I_1\cos\psi)/2$ ($\langle\ \rangle$ denotes time-averaging). A demonstrative picture of the microwave photovoltage mechanism can be seen in Fig. 1.

The second effect we investigate which is also based on AMR spin-charge coupling is the microwave photoresistance ΔR_{MW}. This has been reported recently[13] with the equilibrium magnetization $\mathbf{M}_0$ of a ferromagnetic stripe aligned to a dc current $\mathbf{I}_0$. Microwave induced precession then misaligns the dynamic magnetization **M** with respect to $\mathbf{I}_0$ and thus makes the AMR drop measurably. In this work, we present results which also show that if $\mathbf{M}_0$ lies perpendicular to $\mathbf{I}_0$ the opposite effect takes place: Microwave induced precession causes **M** to leave its perpendicular position which increases the AMR (see Fig. 2).

After this qualitative introduction we want to go ahead with a quantitative description of the AMR induced microwave photovoltage and photoresistance. Therefore, we define an orthogonal coordinate system (x,y,z) (see Fig. 3). The y axis lies normal to the film plane and the z axis is aligned with the magnetic field **H** and hence with the magnetization **M** which is always aligned with **H** in our measurements because of the sample being always magnetized to saturation.

Geometrically our samples are thin films patterned to stripe shape, so that $d \ll w \ll l$, where d, w, and l are the thickness, width, and length of the sample. We apply **H** always in the ferromagnetic film plane. For calculations based on the stripes geometry the coordinates x' and z' are defined. These lie in the film plane. x' is perpendicular and z' parallel to the stripe. The following coordinate transformation applies: $(x,y,z)=[x'\cos(\alpha_0)-z'\sin(\alpha_0),y,z'\cos(\alpha_0)+x'\sin(\alpha_0)]$ where α_0 is the angle between **H** and the stripe.

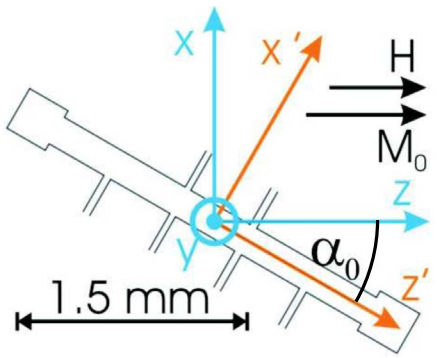

FIG. 3. (Color online) (x,y,z) and (x',y,z') coordinate systems in front of a layout of our Permalloy film stripe ($200\times2400\ \mu\mathrm{m}^2$) with two contacts and six side junctions.

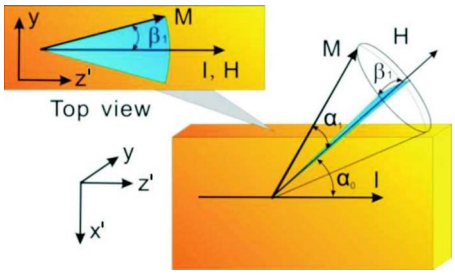

FIG. 4. (Color online) Sketch of the magnetization precession. The magnetic field **H** encloses the angle α_0 with the current **I**. The magnetization oscillation toward **I** has the amplitude α_1 and that perpendicular to **I**: β_1.

For the microwave photovoltage and photoresistance the longitudinal resistance $R(t)=R_0+R_A\cos^2\theta(t)$ of the film stripe matters. It consists of the minimal longitudinal resistance R_0 and the additional resistance $R_A\cos^2\theta(t)$ from AMR. $\theta(t)$ is the angle between the z'-axis (parallel to the stripe) and **M**. **M** moves on a sphere with the radius M_0, which is the saturation magnetization of our sample. $\theta(t)$ can be decomposed into the angle $\alpha(t)$ in the ferromagnetic film plane and the out-of-plane angle $\beta(t)$ (see Fig. 4). Consequently,

$$\cos\theta(t)=\cos\alpha(t)\cos\beta(t). \tag{2}$$

Precession of the magnetization then yields oscillation of $\alpha(t)$, $\beta(t)$, and $\theta(t)$. In our geometry the equilibrium magnetization $\mathbf{M}_0$ encloses the in-plane angle α_0 with the stripe. Hence in time average $\langle\beta(t)\rangle=0$ and $\langle\alpha(t)\rangle=\alpha_0$. In general the magnetization precession is elliptical. Its principle axis lie along the x and y axis and correspond to the amplitudes α_1 and β_1 of the in- and out-of-plane angles α_1^t and β_1^t of the rf magnetization: $\alpha(t)=\alpha_0+\alpha_1^t(t)=\alpha_0+\alpha_1\cos(\omega t-\psi)$ and $\beta(t)=\beta_1^t(t)=-\beta_1\sin(\omega t-\psi)$ [see Fig. 4]. Using Eq. (2) we approximate $\cos^2\theta(t)$ to second order in α_1^t and β_1^t:

$$\cos^2\theta(t)\approx\cos^2\theta|_{\alpha_1^t=\beta_1^t=0}+\alpha_1^t\left.\frac{d\cos^2\theta}{d\alpha_1^t}\right|_{\alpha_1^t=\beta_1^t=0}+0+\frac{\alpha_1^{t2}}{2}\left.\frac{d^2\cos^2\theta}{d\alpha_1^{t2}}\right|_{\alpha_1^t=\beta_1^t=0}+\frac{\beta_1^{t2}}{2}\left.\frac{d^2\cos^2\theta}{d\beta_1^{t2}}\right|_{\alpha_1^t=\beta_1^t=0}. \tag{3}$$

The first order in β_1^t vanishes because it is proportional to $(\sin\beta)|_{\beta_1=0}=0$. It follows that

$$\cos^2\theta(t)\approx\cos^2\alpha_0-\alpha_1\sin 2\alpha_0\cos(\omega t-\psi)-\alpha_1^2\cos 2\alpha_0\cos^2(\omega t-\psi)-\beta_1^2\cos^2\alpha_0\sin^2(\omega t-\psi). \tag{4}$$

This equation is now used to calculate the longitudinal stripe voltage. To consider the general case an externally applied dc current I_0 and a microwave induced rf current I_1 are included in $I(t)=I_0+I_1\cos(\omega t)$. It follows from Eq. (1) that

$$U(t)=[R_0+R_A\cos^2\theta(t)][I_0+I_1\cos(\omega t)]. \tag{5}$$

Consequently $U(t)$ can be written as $U(t)=U_0+U_1\cos(\omega t-\psi_1)+U_2\cos(2\omega t-\psi_2)+U_3\cos(3\omega t-\psi_3)$. For the photovoltage and photoresistance only the constant term U_0, which is equivalent to the time average voltage $\langle U(t)\rangle$, matters. Combining Eqs. (4) and (5), we find

$$U_0=I_0(R_0+R_A\cos^2\alpha_0)-I_1R_A\alpha_1\sin 2\alpha_0\cos(\psi)/2-I_0(\alpha_1^2\cos 2\alpha_0+\beta_1^2\cos^2\alpha_0)R_A/2. \tag{6}$$

Note that $\langle\sin^2(\omega t-\psi)\rangle=\langle\cos^2(\omega t-\psi)\rangle=1/2$ and $\langle\cos\omega t\cos(\omega t-\psi)\rangle=\cos(\psi)/2$. The first term in Eq. (6) is independent of the rf quantities I_1, α_1 and β_1 and represents the static voltage drop of I_0. The second term is the microwave photovoltage U_{MW}. It shows no impact from the dc current I_0. The third term represents the microwave photoresistance ΔR_{MW}. It is proportional to I_0 and depends on the microwave quantities α_1 and β_1. It can be seen now that the rf resistance amplitude R^1 used in the beginning of this paragraph corresponds to $R^1=R_A\alpha_1\sin 2\alpha_0$.

To analyze the magnetization's angle oscillation amplitudes α_1 and β_1 it is necessary to express them by means of the corresponding rf magnetization $\mathrm{Re}(\mathbf{m}e^{-i\omega t})$. **m** is the complex rf magnetization amplitude. Its phase is defined with respect to I_1, so that $\mathrm{Re}(m_xe^{-i\omega t})$ is in phase with $I_1\cos\omega t$ at the FMR. Because $\mathbf{M}=\mathbf{M}_0+\mathbf{m}$, $\mathbf{m}=(m_x,m_y,0)$ can (in first order approximation) only lie perpendicular to $\mathbf{M}_0$ because **M** and $\mathbf{M}_0$ have the same length (M_0). Hence $|m_x|/M_0=\sin\alpha_1\approx\alpha_1$ and $|m_y|/M_0=\sin\beta_1\approx\beta_1$ for $\alpha_1,\beta_1\ll 90°$.

The microwave photovoltage and photoresistance appear whenever magnetization precession is excited. This means if the microwaves are in resonance with the FMR, with standing exchange spin waves perpendicular to the film[10,11,25] or with magnetostatic modes.[11] In this article we will analyze the FMR induced microwave photoresistance and photovoltage.

B. Magnetization dynamics

To understand the impact of the applied rf magnetic field $\mathrm{Re}(\mathbf{h}e^{-i\omega t})$ on the microwave photovoltage and photoresistance the effective susceptibilities χ_{xx}, χ_{xy}, and χ_{yy}, which link $\mathbf{m}e^{-i\omega t}$ inside the sample with the complex external rf magnetic field $\mathbf{h}e^{-i\omega t}=(h_x,h_y,h_z)e^{-i\omega t}$ outside the sample, have to be calculated. Here ψ is encoded in the complex phase of **m**.

The susceptibility inside the sample (magnetic field $\mathbf{h}^{\mathrm{in}}e^{-i\omega t}=(h_x^{\mathrm{in}},h_y^{\mathrm{in}},h_z^{\mathrm{in}})e^{-i\omega t}$) is determined by the Polder tensor[26] $\hat{\chi}$ (received from solving the Landau-Liftshitz-Gilbert equation[28]):

$$\mathbf{m}=\hat{\chi}\mathbf{h}^{\mathrm{in}}=\begin{pmatrix}\chi_L & i\chi_T & 0\\ -i\chi_T & \chi_L & 0\\ 0 & 0 & 0\end{pmatrix}\mathbf{h}^{\mathrm{in}}, \tag{7}$$

with

$$\chi_L = \frac{\omega_M \omega_r}{\omega_r^2 - \omega^2}, \quad \chi_T = \frac{\omega \omega_M}{\omega_r^2 - \omega^2},$$

where $\omega_M = \gamma M_0$ with the gyromagnetic ratio $\gamma \approx \mu_0 \times e/m = 2\pi\mu_0 \times 28$ GHz/T (electron charge e and mass m_e) and $\omega_r = \gamma H$ without damping. Approximation of our sample as a two-dimensional film results in the boundary conditions that h_x and b_y are continuous at the film surface meaning $h_x = h_x^{\text{in}}$ and $b_y = \mu_0 h_y = \mu_0[(1+\chi_L)h_y^{\text{in}} - i\chi_T h_x^{\text{in}}]$. Hence

$$\mathbf{m} = \begin{pmatrix} \chi_{xx} & i\chi_{xy} & 0 \\ -i\chi_{xy} & \chi_{yy} & 0 \\ 0 & 0 & 0 \end{pmatrix} \mathbf{h}, \tag{8}$$

with

$$\chi_{xx} = \frac{\omega_r \omega_M + \omega_M^2}{\omega_r(\omega_r + \omega_M) - \omega^2},$$

$$\chi_{xy} = \frac{\omega \omega_M}{\omega_r(\omega_r + \omega_M) - \omega^2},$$

$$\chi_{yy} = \frac{\omega_r \omega_M}{\omega_r(\omega_r + \omega_M) - \omega^2}.$$

χ_{xx} is identical to the susceptibility describing the propagation of microwaves in an unlimited ferromagnetic medium in Voigt geometry[29] (propagation perpendicular to $\mathbf{M}_0$). χ_{xx}, χ_{xy}, and χ_{yy} have the same denominator, which becomes resonant (maximal) when $\omega = \sqrt{\omega_r^2 + \omega_r \omega_M}$. This is in accordance with the FMR frequency of the Kittel formula for in-plane magnetized infinite ferromagnetic films.[30]

This relatively simple behavior is due to the assumption that $\mathbf{h}^{\text{in}}$ is constant within the film stripe. This assumption is only valid if the skin depth[1] δ of the microwaves in the sample is much larger than the sample thickness. During our measurements we fix the microwave frequency f and sweep the magnetic field H. Consequently we find the FMR magnetic field H_0 with

$$\omega^2 = \gamma^2(H_0^2 + H_0 M_0) \tag{9}$$

and

$$H_0 = \sqrt{M_0^2/4 + \omega^2/\gamma^2} - M_0/2. \tag{10}$$

Now we introduce Gilbert damping[27] α_G by setting $\omega_r := \omega_0 - i\alpha_G\omega$ with now $\omega_0 = \gamma H$ instead of $\omega_r = \gamma H$. We separate the real and imaginary part of χ_{xx}, χ_{xy}, and χ_{yy}:

$$\chi_{xx} = (\omega_r \omega_M + \omega_M^2)F,$$

$$\chi_{xy} = \omega \omega_M F,$$

$$\chi_{yy} = \omega_r \omega_M F, \tag{11}$$

with

$$F = \frac{\omega_0(\omega_0 + \omega_M) - \alpha_G^2\omega^2 - \omega^2 + i\alpha_G\omega(2\omega_0 + \omega_M)}{[\omega_0(\omega_0 + \omega_M) - \alpha_G^2\omega^2 - \omega^2]^2 + \alpha_G^2\omega^2(2\omega_0 + \omega_M)^2}$$

$$\approx \frac{(H + H_0 + M_0)(H - H_0) + i(2H + M_0)\alpha_G\omega/\gamma}{(H + H_0 + M_0)^2(H - H_0)^2 + (2H + M_0)^2\alpha_G^2\omega^2/\gamma^2}.$$

The approximation was done by neglecting the $\alpha_G^2\omega^2$ correction to the resonance frequency $\omega^2 = \omega_0(\omega_0 + \omega_M) - \alpha_G^2\omega^2 \approx \omega_0(\omega_0 + \omega_M)$ which is possible if $\alpha_G \ll 1$. Hence

$$\chi_{xx,xy,yy} \approx A_{xx,xy,yy} \frac{\Delta H(H - H_0) + i\Delta H^2}{(H - H_0)^2 + \Delta H^2}, \tag{12}$$

with $\Delta H = [(2H + M_0)/(H + H_0 + M_0)]\alpha_G\omega/\gamma$. This can be approximated as $\Delta H \approx \alpha_G\omega/\gamma$ if $|H - H_0| \ll H_0$. A_{xx}, A_{xy}, and A_{yy} determine the scalar amplitude of χ_{xx}, χ_{xy}, and χ_{yy}.

To analyze the FMR line shape in the following, we will call the Lorentz line shape which is proportional to $\Delta H/[(H - H_0)^2 - \Delta H^2]$ symmetric Lorentz line shape and the line shape proportional to $(H - H_0)/[(H - H_0)^2 - \Delta H^2]$ antisymmetric Lorentz line shape. A linear combination of both will be called asymmetric Lorentz line shape. $|H - H_0| \ll H_0$ allows us to approximate

$$A_{xx} \approx \frac{\gamma(H_0 M_0 + M_0^2)}{\alpha_G\omega(2H_0 + M_0)},$$

$$A_{xy} \approx \frac{M_0}{\alpha_G(2H_0 + M_0)},$$

$$A_{yy} \approx \frac{\gamma H_0 M_0}{\alpha_G\omega(2H_0 + M_0)}. \tag{13}$$

These are scalars which are independent of the dc magnetic field H and hence characteristic for the sample at fixed frequency. Indeed the assumption of Gilbert damping is not essential for the derivation of Eq. (13). In the event of a different kind of damping, ΔH can also be directly input into Eq. (13) replacing $\alpha_G\omega$. However, because of the commonness of Gilbert damping, its usage here can provide a better feeling for the usual frequency dependence of $A_{xx,xy,yy}$. Going ahead, Eq. (8) becomes

$$\mathbf{m} \approx \frac{\Delta H(H - H_0) + i\Delta H^2}{(H - H_0)^2 + \Delta H^2} \begin{pmatrix} A_{xx} & iA_{xy} & 0 \\ -iA_{xy} & A_{yy} & 0 \\ 0 & 0 & 0 \end{pmatrix} \mathbf{h}. \tag{14}$$

The H-field dependencies has Lorentz line shape with antisymmetric (dispersive) real and symmetric (absorptive) imaginary part, the amplitudes A_{xx}, $\pm iA_{xy}$, and A_{yy}, respectively, and the width ΔH. Note that $A_{xx}A_{yy} \approx A_{xy}^2$ for $|H - H_0| \ll H_0$. Consequently, the susceptibility amplitude tensor can be simplified to

$$\begin{pmatrix} A_{xx} & iA_{xy} & 0 \\ -iA_{xy} & A_{yy} & 0 \\ 0 & 0 & 0 \end{pmatrix} \mathbf{h} \approx \begin{pmatrix} \sqrt{A_{xx}} \\ -i\sqrt{A_{yy}} \\ 0 \end{pmatrix} \left[\begin{pmatrix} \sqrt{A_{xx}} \\ i\sqrt{A_{yy}} \\ 0 \end{pmatrix} \mathbf{h} \right]$$

and Eq. (14) becomes

$$\mathbf{m} = \frac{\gamma M_0}{\alpha_G \omega(2H_0 + M_0)} \frac{\Delta H(H - H_0) + i\Delta H^2}{(H - H_0)^2 + \Delta H^2} \begin{pmatrix} \sqrt{1 + M_0/H_0} \\ -i \\ 0 \end{pmatrix} \times \left[\begin{pmatrix} \sqrt{1 + M_0/H_0} \\ i \\ 0 \end{pmatrix} \mathbf{h} \right]. \quad (15)$$

It is visible that the ellipticity of **m** is independent of the exciting magnetic field **h**. Only the amplitude and phase of **m** are defined by **h**. The reason is the weak Gilbert damping α_G for which much energy needs to be stored in the magnetization precession to have a compensating dissipation. Hence little energy input and impact from **h** appears.

From Eq. (15) follows that m_x and m_y have cardinally the ratio

$$m_x/m_y = i\sqrt{1 + M_0/H_0}. \quad (16)$$

Therefore, m_y vanishes for $\omega \to 0$ and $m_x = im_y$ for $\omega \to \infty$. This means that the precession of **M** is elliptical and becoming more circular for high frequencies and more linear (along the x axis) for low frequencies. This description applies for the case of an in-plane magnetized ferromagnetic film. However, in the case that the sample has circular symmetry with respect to the magnetization direction (e.g., in a perpendicular magnetized disk or infinite film[10,11]): $\alpha_1 = \beta_1$. This is the same as in the case that $\omega \to \infty$. Only in these cases the magnetization precession can be described in terms of one precession cone angle.[13] Otherwise, distinct attention has to be paid to α_1 and β_1 (see III B). Additionally, it can be seen in Eq. (15) that m_y/m_x is also the ratio of the coupling strength of **m** to h_y and h_x, respectively.

C. Microwave photoresistance

The microwave photoresistance ΔR_{MW} can be deduced from Eq. (6). First the microwave photovoltage is excluded by setting the rf current $I_1 = 0$. Then we only regard the microwave power dependent terms which depend on α_1 and β_1:

$$\Delta R_{\mathrm{MW}} = (U_0|_{I_1=0} - U_0|_{I_1=0,\alpha_1=0,\beta_1=0})/I_0 = R_A(-\alpha_1^2 \cos 2\alpha_0 - \beta_1^2 \cos^2\alpha_0)/2. \quad (17)$$

If the magnetization lies parallel or antiparallel to the dc current vector $\mathbf{I}_0$ along the stripe ($\alpha_0 = 0°$ or $\alpha_0 = 180°$) the AMR is maximal. In this case magnetization oscillation (α_1 and β_1) reduces ($-\cos 2\alpha_0 = -1$) the AMR by $\Delta R_{\mathrm{MW}} = -(\alpha_1^2 + \beta_1^2)R_A/2$ (negative photoresistance). In contrast, if the magnetization lies perpendicular to $\mathbf{I}_0$ ($\alpha_0 = 90°$, see Fig. 2) the resistance is minimal. In this case magnetization oscillation corresponding to α_1 will increase ($-\cos 2\alpha_0 = +1$) the AMR (positive photoresistance) by $\Delta R_{\mathrm{MW}} = +\alpha_1^2 R_A/2$ [oscillations corresponding to $\beta_1$leave $\theta(t)$ constant in this case and do not change the AMR].

The next step is to calculate α_1 and β_1. The dc magnetic field dependence of $\alpha_1 = |m_x|/M_0 = |\chi_{xx}h_x + i\chi_{xy}h_y|/M_0$ and $\beta_1 = |m_y|/M_0 = |-i\chi_{xy}h_x + \chi_{yy}h_y|/M_0$ is proportional to that of $|\chi_{xx}|$, $|\chi_{xy}|$, and $|\chi_{yy}|$ given in Eq. (12) (imaginary symmetric and real antisymmetric Lorentz line shape). Squaring this results in symmetric Lorentz line shape:

$$\alpha_1^2 \propto \beta_1^2 \propto \left| \frac{\Delta H(H - H_0) + i\Delta H^2}{(H - H_0)^2 + \Delta H^2} \right|^2 = \frac{\Delta H^2}{(H - H_0)^2 + \Delta H^2}.$$

Hence

$$\alpha_1^2 = \frac{|A_{xx}h_x + iA_{xy}h_y|^2}{M_0^2} \frac{\Delta H^2}{(H - H_0)^2 + \Delta H^2},$$

$$\beta_1^2 = \frac{|A_{yy}h_y - iA_{xy}h_x|^2}{M_0^2} \frac{\Delta H^2}{(H - H_0)^2 + \Delta H^2}. \quad (18)$$

Using Eqs. (15) and (18), Eq. (17) transforms to

$$\Delta R_{\mathrm{MW}} = \frac{R_A}{(\alpha_G \omega/\gamma)^2(2H_0 + M_0)^2}[-(H_0 + M_0)\cos 2\alpha_0 - H_0 \cos^2\alpha_0] \frac{\Delta H^2}{(H - H_0)^2 + \Delta H^2} \times |h_x\sqrt{H_0 + M_0} + ih_y\sqrt{H_0}|^2. \quad (19)$$

The strength of the microwave photoresistance is proportional to $1/\alpha_G^2$. Weak damping (small α_G) is therefore critical for a signal strength sufficient for detection. The magnetic field dependence shows symmetric Lorentz line shape.

The dependence of ΔR_{MW} on α_0 in Eq. (19) reveals a sign change and hence vanishing of the photoresistance at

$$\cos^2\alpha_0 = \frac{1}{2}\left(1 - \frac{H_0}{3H_0 + 2M_0}\right). \quad (20)$$

This means that the angle at which the photoresistance vanishes shifts from $\alpha_0 = \pm 45°$ and $\alpha_0 = \pm 135°$ (for $\omega \to 0$) to $\alpha_0 = \pm 54.7°$ and $\alpha_0 = \pm 125.3°$ respectively (for $\omega \to \infty$) when increasing ω. The reason for this frequency dependence is the frequency dependence of the ellipcity of **m** described at the end of Sec. II B.

D. Microwave photovoltage

The most obvious difference in appearance between the microwave photoresistance discussed in Sec. II C and the microwave photovoltage discussed in this paragraph is that the photoresistance is proportional to the square of the rf magnetization [see Eq. (17), $\alpha_1^2 \approx |m_x|^2/M_0^2$ and $\beta_1^2 \approx |m_y|^2/M_0^2$] while the photovoltage U_{MW} is proportional to the product of the rf magnetization and the rf current. Consequently, the photovoltage has a very different line shape: While the rf magnetization depends with Lorentz line shape on H [see Eq. (12)], I_1 is independent of H. The line shape is hence determined by the phase difference ψ between the rf magnetization component $\mathrm{Re}(m_x e^{-i\omega t})$ and the rf current $I_1 \cos \omega t$. This effect does not play a role in the case of photoresistance because there only one phase matters namely that of the rf magnetization. In contrast in photovoltage measurements a linear combination of symmetric and antisymmetric Lorentz line shapes is found. This will be discussed in detail in the following.

To isolate the microwave photovoltage in Eq. (6) the dc current I_0 is set to 0:

$$U_{\mathrm{MW}} = U_0|_{I_0=0} = -I_1\alpha_1\frac{R_A \sin 2\alpha_0 \cos\psi}{2}. \tag{21}$$

From Eq. (8) we follow with

$$\alpha_1 \cos\psi = \mathrm{Re}(m_x) = \mathrm{Re}(\chi_{xx}h_x + i\chi_{xy}h_y). \tag{22}$$

We split $h_x = h_x^r + ih_x^i$ and $h_y = h_y^r + ih_y^i$ into real (h_x^r, h_y^r) and imaginary (h_x^i, h_y^i) part. This enables us to isolate the real part in Eq. (21) using Eq. (14):

$$U_{\mathrm{MW}} = \frac{I_1 R_A \sin 2\alpha_0}{2M_0}\left\{\frac{(A_{xy}h_y^r + A_{xx}h_x^i)\Delta H^2}{(H-H_0)^2+\Delta H^2} + \frac{(A_{xy}h_y^i - A_{xx}h_x^r)\Delta H(H-H_0)}{(H-H_0)^2+\Delta H^2}\right\}. \tag{23}$$

Conclusively in contrast to the microwave photoresistance [$\Delta R_{\mathrm{MW}} \propto 1/\alpha_G^2$, see Eq. (19)] the photovoltage is only proportional to $1/\alpha_G \propto A_{xx,xy,yy}$. Thus good damping is less important for its detection.[31]

To understand the measurement results it will be necessary to transform the coordinate system of Eq. (23) to (x', y, z'). In this coordinate system the rf magnetic field **h** is constant during rotation as described in Eq. (33).

To better understand the photovoltage line shape we have a closer look on ψ: When sweeping H the rf magnetization phase is shifted by ψ_m with respect to the resonance case ($H=H_0$). The rf current has a constant phase ψ_I which is defined with respect to the magnetization's phase at resonance. The impact of the dc magnetic field H on the rf current (I_1, ψ_I) via the FMR is believed to be negligible:

$$\cos\psi = \cos(\psi_m - \psi_I) = \cos\psi_m \cos\psi_I + \sin\psi_m \sin\psi_I. \tag{24}$$

ψ is determined by the (complex) phase of χ_{xx}, χ_{xy}, and χ_{yy} with respect to the resonance case [$\mathrm{Re}(\chi_{xy,yy})=0$ at $H=H_0$] during magnetic field sweep [asymmetric Lorentz line shape; see Eq. (12)]:

$$\tan\psi_m = \frac{\mathrm{Im}\left(\frac{\Delta H(H-H_0)+i\Delta H^2}{(H-H_0)^2+\Delta H^2}/i\right)}{\mathrm{Re}\left(\frac{\Delta H(H-H_0)+i\Delta H^2}{(H-H_0)^2+\Delta H^2}/i\right)} = \frac{H_0-H}{\Delta H}. \tag{25}$$

It should be noted that according to the Landau-Liftshitz equation[28] **h** applies a torque on the magnetization and hence excites $\mathbf{m}^t$ transversal. That is why at resonance m_x shows a phase shift of 90° with respect to h_x. Consequently in Eq. (25) division by i is necessary (χ_{xx} and χ_{xy} become imaginary at resonance).

Equation (25) means that in case that the applied microwave frequency is higher than the FMR frequency ($H_0 > H$) $\psi_m > 0$ (note that $\mathbf{m}^t = \mathbf{m}e^{-i\omega t}$), $\mathbf{m}^t$ is delayed with respect to the resonant case. The other way around ($H_0 < H$) the FMR frequency is higher than that of the applied microwave field and $\mathbf{m}^t$ is running ahead compared to the resonance case. Using Eq. (25) we find

$$\cos\psi_m = \frac{\Delta H}{\sqrt{(H-H_0)^2+\Delta H^2}}. \tag{26}$$

Inserting Eqs. (18) and (24)–(26) into Eq. (21) gives

$$U_{\mathrm{MW}} = -\frac{R_A I_1 \sin 2\alpha_0}{2}\frac{|A_{xx}h_x + iA_{xy}h_y|}{M_0}\left(\frac{\Delta H^2 \cos\psi_I}{(H-H_0)^2+\Delta H^2} - \frac{(H-H_0)\Delta H \sin\psi_I}{(H-H_0)^2+\Delta H^2}\right). \tag{27}$$

The dependence on H takes the form of a linear combination of symmetric and antisymmetric Lorentz line shape with the ratio $1:\tan\psi_I$. The symmetric line shape contribution ($\propto \Delta H$) arises from the rf current contribution that is in phase with the rf magnetization at FMR and the antisymmetric from that out-of-phase. This gives a nice impression of the phase ψ_I of the rf current determining the line shape of the FMR.

E. Vectorial description of the photovoltage

To complete the discussion of the microwave photovoltage we want to return to the approach used by Juretschke[23] to demonstrate that it is consistent with the description above. In Sec. II A we started with Ohm's law [scalar equation (1)]. There we integrate an angle- and time-dependent resistance. Here we want to start with the vectorial notation of Ohm's law used in Juretschke's publication [Eq. (1) (Ref. 23)]. This integrates AMR and anomalous Hall effect AHE. ρ is the resistivity of the sample and $\Delta\rho$ that additionally arising from AMR. R_H is the anomalous Hall effect constant:

$$\mathbf{E} = \rho\mathbf{J} + (\Delta\rho\mathbf{M}^2)(\mathbf{J}\cdot\mathbf{M})\mathbf{M} - R_H\mathbf{J}\times\mathbf{M}. \tag{28}$$

We split $\mathbf{M} = \mathbf{M}_0 + \mathbf{m}^t$ and the current density $\mathbf{J} = \mathbf{J}_0 + \mathbf{j}^t$ into their dc ($\mathbf{M}_0$ and $\mathbf{J}_0$) and rf contributions [$\mathbf{m}^t = \mathrm{Re}(\mathbf{m}e^{-i\omega t})$ and $\mathbf{j}^t = \mathbf{j}\cos\omega t$]. Constance of $|\mathbf{M}|$ allows $\mathbf{m}^t = (m_x^t, m_y^t, 0)$ in first order approximation only to lie perpendicular to $\mathbf{M}_0 = (0,0,M_0)$. To select the photovoltage we set $\mathbf{J}_0 = 0$ and approximate equation (28) to second order in $\mathbf{j}^t$ and $\mathbf{m}^t$. The terms of zeroth order in both $\mathbf{j}^t$ and $\mathbf{m}^t$ represent the sample resistance without microwave exposure and are not discussed here. The terms of first order in either $\mathbf{j}^t$ or $\mathbf{m}^t$ (but not both) have zero time average and do not contribute to the microwave induced dc electric field $\mathbf{E}_{\mathrm{MW}}$. Only the terms that are simultaneously of first order in $\mathbf{j}^t$ and $\mathbf{m}^t$ contribute to $\mathbf{E}_{\mathrm{MW}}$ [compare Eq. (4) from Juretschke[23]]:

$$\mathbf{E}_{\mathrm{MW}} = \frac{\Delta\rho}{M_0^2}\langle(\mathbf{j}^t\mathbf{m}^t)\mathbf{M}_0 + (\mathbf{j}^t\mathbf{M}_0)\mathbf{m}^t\rangle - R_H\langle\mathbf{j}^t\times\mathbf{m}^t\rangle. \tag{29}$$

The $\Delta\rho$ dependent term represents the photovoltage contribution arising from AMR and the R_H dependent term that arising from AHE. Note that a second order of $\mathbf{m}^t$ appears when applying a dc current $\mathbf{J}_0 \neq 0$. It represents the photoresistance discussed in Sec. II C. However, it we will not be discussed here.

In the following we will calculate the photovoltage in our Permalloy film stripe considering its geometry which fixes the current direction. $\mathbf{j}^t = j_{z'}^t\mathbf{z}'$ along the stripe ($\mathbf{z}'$ is the unit

vector along the Permalloy stripe). The small dimensions perpendicular to the stripe ($\ll L$) will prevent the formation of a perpendicular rf current. A similar approximation of a metal grating forming a linear polarizer has been considered previously.[9] The photovoltage U_{MW} is also measured along the stripe (length vector $\mathbf{L}=\mathbf{z}'\times 2.4$ mm). When fluctuations of $\mathbf{E}_{\mathrm{MW}}$ along the stripe are neglected considering the large microwave wavelength, $\lambda \approx 20\ \mathrm{mm} \gg 2.4\ \mathrm{mm}=L$, we find U_{MW} by multiplying $\mathbf{E}_{\mathrm{MW}}$ with $\mathbf{L}$:

$$U_{\mathrm{MW}} = \int_0^L \mathbf{E}_{\mathrm{MW}} d\mathbf{z}' \approx \mathbf{E}_{\mathrm{MW}} \cdot \mathbf{L}$$

$$= \frac{\Delta\rho L}{M_0^2}\langle j_{z'}^t(\mathbf{z}'\mathbf{m}^t)(\mathbf{M}_0\mathbf{z}') + j_{z'}^t(\mathbf{z}'\mathbf{M}_0)(\mathbf{m}^t\mathbf{z}')\rangle - 0$$

$$= \frac{\Delta\rho L}{M_0}\langle j_{z'}^t m_x^t\rangle \sin(2\alpha_0). \tag{30}$$

This is equivalent to Eq. (21) which can be verified by replacing $\Delta\rho j_{z'}^t L = R_A I_1 \cos(\omega t)$ and $m_x^t = \alpha_1 M_0 \cos(\omega t - \psi)$. Time averaging results in the additional factor $\cos(\psi)/2$.

As discussed in Sec. II F the contribution belonging to the anomalous Hall effect has no impact in this geometry because it can only generate a photovoltage perpendicular to the rf current, i.e., perpendicular to the stripe.

Comparing our results to those of Juretschke and Egan,[23,31] we note that an equation similar to Eq. (30) has been derived in the formula for e_{y0} in Eq. (31) in Juretschke's publication.[23] There the photovoltage is measured parallel to the rf current as done in our stripe. However, it has to be noted that the coordinate system is defined differently. The major difference compared to our system is that we use a stripe shaped film to lithographically define the direction of the rf current I_1, while the direction of $\mathbf{h}$ is left arbitrary. In contrast to that, Juretschke and Egan[23,31] define the direction of the rf magnetic field and rf current by means of their microwave setup. In Eq. (31) (e_{y0}) from Juretschke[23] this results in the additional factor $\cos\theta$ (which is equivalent to $\cos\alpha_0$ in our work) compared to Eq. (30). This arises from the definition of $\mathbf{h}$ fixed parallel to the rf current [compare Eq. (33)].

F. Other magnetoresistive effects that couple spin and charge current

In this section we present other magnetoresistive effects which can generate photovoltage and photoresistance like the AMR. This selection gives a broader view on the range of effects for which the photovoltage and photoresistance can be discussed in terms of the analysis presented in this work. In principle every magnetoresistive effect can modulate the sample resistance and thus rectify some of the rf current to photovoltage.

One magnetoresistive effect is the anomalous Hall effect AHE in ferromagnetic metals that was (together with the AMR) the basis for the discussion of Juretschke.[23] There a current with perpendicular magnetization generates a voltage perpendicular to both. Under microwave exposure this alternates with the microwave frequency but in an asymmetric way due to the modulated AHE arising from magnetization precession. The asymmetric voltage has a dc contribution (photovoltage),[31] which can be measured using a two-dimensional ferromagnetic film with the magnetization neither parallel nor perpendicular to it. The photovoltage induced by AHE appears in the film plane perpendicular to the rf current and is small[25] for Permalloy ($Ni_{80}Fe_{20}$). Also a photoresistive effect which alters the AHE can be expected if the magnetization lies out-of-plane.

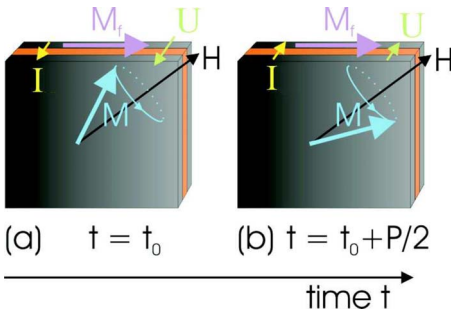

FIG. 5. (Color online) Microwave photovoltage in a GMR/TMR heterostructure [ferromagnetic (**M**)/nonferromagnetic/ferromagnetic ($\mathbf{M}_f$)]: The dynamic magnetization **M** precesses (period P) in phase with the current **I**. (a) **M** lies almost perpendicular to $\mathbf{M}_f$: High GMR/TMR. (b) **M** lies almost parallel to $\mathbf{M}_f$: Low GMR/TMR $\Rightarrow$ nonzero time average of the voltage **U**.

Other examples for magnetoresistive effects are GMR and TMR structures which exhibit a photovoltage mechanism similar to that in AMR films. The difference is that there the direction of the ferromagnetic layer magnetization with respect to the current does not matter. Effectively instead the direction of the magnetization **M** of one ferromagnetic layer with respect to that of another layer is decisive (see Fig. 5). Exciting the FMR in one layer yields again oscillation of the sample resistance $R(t)$ and thus gives the corresponding rf voltage $U(t)$ a nonzero time average (photovoltage).[4,32] This is usually stronger than that from AMR films due to the generally higher relative strength of GMR and TMR compared to AMR.

It should be noted that in current studies of the microwave photovoltages effect in multilayer structures, the focus is on interfacial spin transfer effects.[4–8,19–21,32] It remains an intriguing question whether interfacial spin transfer effects and the effect revealed in our approach based on phenomenological magnetoresistance might be unified by a consistent microscopic model, as Silsbee *et al.* have demonstrated for describing both bulk and interfacial spin transport under rf excitation.[24]

Multilayer structures also provide a nice example that photovoltage generation can also be reversed when the oscillating magnetoresistance, transforms a dc current into an rf voltage,[33] instead of transforming an rf current into a dc voltage (photovoltage). This gives a new kind of microwave source and seems—although weaker—also possible in AMR and AHE samples.

It can be reasoned that like microwave photovoltage the microwave photoresistance can also be based on GMR or TMR instead of AMR: When aligning the two magnetiza-

tions of both ferromagnetic layers in a GMR or TMR structure microwave induced precession of one magnetization is expected to increase the GMR/TMR because of the arising misalignment with the other magnetization. With the magnetizations initially antiparallel the opposite effect, a microwave induced resistance decrease, is expected. Further work demonstrating these effects would be interesting.

III. PHOTOVOLTAGE MEASUREMENTS

A. Measurement setup

The sample we use to investigate the microwave photovoltage consists of a thin (d=49 nm) Permalloy (Ni 80%, Fe 20%) film stripe (200 μm wide and 2400 μm long) with 300×300 μm^2 bond pads at both ends (see Fig. 3). These are connected via gold bonding wires and coaxial cables to a lock-in amplifier. For auxiliary measurements (e.g., Hall effect) six additional junctions are attached along the stripe (see Fig. 3).

The resistance of the film stripe is $R_0+R_A=85.0\ \Omega$ for parallel and $R_0=83.6\ \Omega$ for perpendicular magnetization. Hence the conductance is $\sigma=1/\rho=2.9\times10^6\ \Omega^{-1}\ \mathrm{m}^{-1}$ and the relative AMR is $\Delta\rho/\rho=1.7\%$. The absolute AMR is $R_A=1.4\ \Omega$. This is in good agreement with previous publications.[9–11]

The film is deposited on a 0.5 mm thick GaAs single crystal substrate, and patterned using photolithography and lift off techniques. The substrate is mounted on a 1 mm polyethylene print circuit board which is glued to a brass plate holding it in between the poles of an electromagnet. This provides the dc magnetic field $B=\mu_0 H$ (maximal $\approx$1 T). The sample is fixed 1 mm behind the end of a WR62 (15.8 $\times$7.9 mm) hollow brass waveguide which is mounted normal to the Permalloy film plane. The stripe is fixed along the narrow waveguide dimension. In the K_u band (12.4–18 GHz), that we use in our measurements, the WR62 waveguide only transmits the TE_{01} mode.[1] The stripe was fixed with respect to the waveguide but was left rotatable with respect to **H**. This allows the stripe to be parallel or perpendicular to **H**, but keeps the magnetic field always in the film plane. A high precision angle readout was installed to indicate α_0. (See Fig. 6).

The waveguide is connected to an HP83624B microwave generator by a coaxial cable supplying frequencies of up to 20 GHz and a power of 200 mW. The power is however later significantly reduced by losses occurring within the coaxial cable, during the transfer to the hollow waveguide and by reflections at the end of the waveguide. Microwave photovoltage measurements are performed sweeping the magnetic field while fixing the microwave frequency. The sample is kept at room temperature.

To avoid external disturbances the photovoltage was detected using a lock-in technique: A low frequency (27.8 Hz) square wave signal is modulated on the microwave CW output. The lock-in amplifier, connected to the Permalloy stripe, is triggered to the modulation frequency to measure the resulting square wave photovoltage across the sample. Instead of the photovoltage also the photocurrent can be measured.[10]

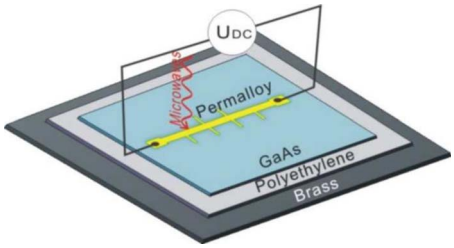

FIG. 6. (Color online) Sketch of the measurement geometry. A 1 mm thick polyethylene plate is glued on a brass holder. On top of the polyethylene a GaAs substrate is glued. On the substrate the Permalloy (Py) stripe is defined. This is electrically wired to a voltage amplifier for photovoltage measurements. For photoresistance measurements an additional current source is connected parallel to the voltage amplifier, which is not shown explicitly here.

Its strength I_0 can be found when setting $U_0=0$ in Eq. (6) (instead of $I_0=0$).

B. Ferromagnetic resonance

The measured photovoltage almost vanishes during most of the magnetic field sweep but shows one pronounced resonance of several μV. The strength and line shape of this resonance are strongly depending on α_0 and will be discussed in Sec. III C. A line shape dependence of the photovoltage on the microwave frequency is also found. The photovoltage with respect to the strength of the external magnetic field H and the microwave frequency $f=\omega/2\pi$ can be seen in a gray scale plot in Fig. 7, in which the resonance can be identified with the FMR by the corresponding fits (dashed line) because the Kittel equation (9) (Ref. 30) for ferromagnetic planes (our Permalloy film) applies. The magnetic parameters found are $\mu_0 M_0\approx1.02$ T and $\gamma\approx2\pi\mu_0\times28.8$ GHz/T. They are in good agreement with previous publications.[9,10]

The exact position of the FMR is obscured by its strongly varying line shape. We overcome this problem by the pro-

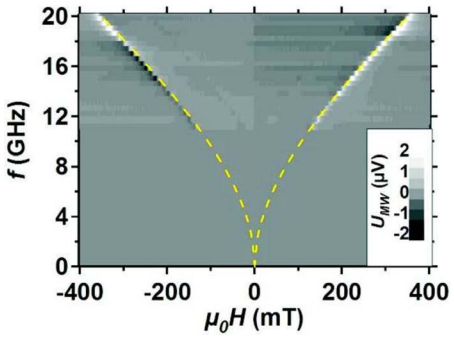

FIG. 7. (Color online) Gray scale plot of the measured frequency and magnetic field dependence of the microwave photovoltage at $\alpha_0=47°$. The dashed line shows the calculated FMR frequency [see Eq. (9)]. The photovoltage intensity is strongly frequency dependent because of the frequency dependent waveguide transmission.

ductive line shape analysis in Sec. III C. It is found that H_0 is slightly dependent on α_0. This can be attributed to a small demagnetization field perpendicular to the stripes but within the film plane arising from the finite stripe dimensions in this direction. So, when $\mathbf{M}_0$ lies perpendicular to the stripe, H_0 slightly increases compared to the value fulfilling the Kittel equation for a plane [see Eq. (9)]. In the parallel and perpendicular case we use the approximation of our film stripe as an ellipsoid, where we can use the corresponding Kittel equation[30] (demagnetization factors N_x, N_y, and N_z with respect to the dc magnetic field):

$$\omega = \gamma\sqrt{[H_0 + (N_x - N_z)M_0][H_0 + (N_y - N_z)M_0]}. \quad (31)$$

The difference of the resonance field between the case that $\mathbf{M}_0$ lies in the film plane parallel to the stripe and perpendicular is 1.6 mT (0.7%) at $f=15$ GHz. From this we can calculate the small demagnetization factor $N_{x'}=0.085\%$ perpendicular to the Permalloy stripe within the film plane using Eq. (31). From the sum rule[34] follows: $N_y=1-N_{x'}-N_{z'}=1-0.085\%-0=99.915\%$. $N_{z'}$ (parallel to the stripe) can be assumed to be negligibly small. This matches roughly with the dimension of the height to width ratio (49 nm:200 μm) of the sample. For the stripe presented in Sec. IV similar but stronger demagnetization effects are found.

Now we will have a closer look on the magnetic properties of the investigated film. Again at $f=15$ GHz we find using Eq. (10): $H_0=0.219$ T. Using asymmetric Lorentz line shape fitting as described in Sec. III C we get $\alpha_G=0.0072$. Consequently, $A_{xx}=231.1$, $A_{xy}=97.1$, and $A_{yy}=40.8$ according to Eq. (13).

Because of $\alpha_G=0.0072$ the magnetization precession does impressive $n\approx 22$ turns before being damped to $1/e$ of its initial amplitude ($n=1/2\pi\alpha_G$). Therefore the ellipcity of $\mathbf{m}$ is almost independent of $\mathbf{h}$ (see Sec. II B). It can be calculated from Eq. (16) that $m_x/m_y=2.38i$ at $\omega/2\pi=15$ GHz.

To check the validity of our approximation ($d \ll \delta$, see Sec. II B) we will now regard the skin depth δ at $f=15$ GHz in our sample ($d=49$ nm). For $\mu=\mu_0$ (away from the FMR) we find $\delta=\sqrt{2/\omega\mu\rho}=2.4$ μm. Hence $\delta \gg d$. This is in accordance with our approximation that $\mathbf{h}$ is almost constant within the Permalloy film (see II B). However, in the vicinity of the FMR: $|\mu| \gg \mu_0$ and for the same frequency and conditions as above: $\mu_L=(1+\chi_L)\mu_0=133i\mu_0$ at the FMR. Thus we approximate $\delta_{\mathrm{FMR}}=\sqrt{2/\omega|\mu_L|\rho}=210$ nm. Hence δ_{FMR} is still significantly larger than d and our approximation is still valid.

Finally we can summerize that for samples with weak damping ($\alpha_G \ll \omega/\omega_M$) like ours the approximation $H\approx H_0$ gives results with impressive precision (see Fig. 8) because its discrepancies are limited to the unimportant magnetic field ranges with $|\chi_{xx}|$, $|\chi_{xy}|$, and $|\chi_{yy}| \ll 1$, which are far away from the FMR.

C. Asymmetric Lorentz line shape

Although in Sec. III B the frequency dependence of the FMR field is verified with the gray scale plot in Fig. 7, it is still desirable to receive a more accurate picture of the corresponding line shape which is found to be strongly angular dependent (see Fig. 8). In Eq. (27) it is shown that the magnetic field dependence of U_{MW} exhibits asymmetric Lorentz line shape around $H=H_0$. Hence U_{MW} takes the form

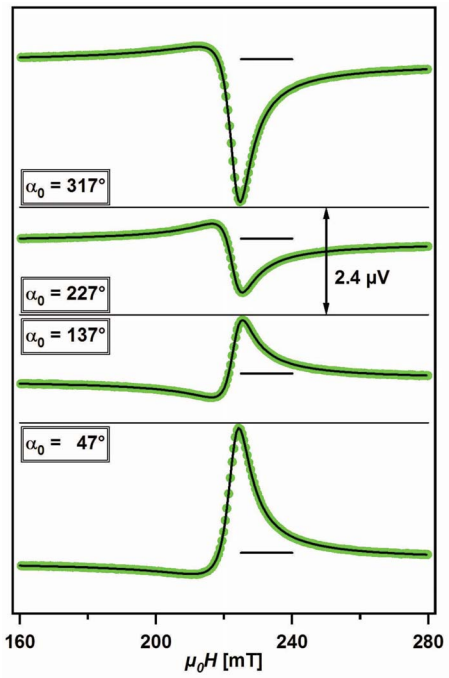

FIG. 8. (Color online) Fitting (black line) of the microwave photovoltage signal (dots) for different angles α_0 at $f=15$ GHz. The black horizontal bars indicate zero signal.

$$U_{\mathrm{MW}} = U_{\mathrm{MW}}^{\mathrm{SYM}} + U_{\mathrm{MW}}^{\mathrm{ANT}} = U_0^{\mathrm{SYM}}\frac{\Delta H^2}{(H-H_0)^2+\Delta H^2} + U_0^{\mathrm{ANT}}\frac{\Delta H(H-H_0)}{(H-H_0)^2+\Delta H^2}. \quad (32)$$

This is used to fit the magnetic field dependence of the photovoltage in Fig. 8. For clearness the symmetric (absorptive) and antisymmetric (dispersive) contributions are shown separately in Fig. 9. A small constant background is found and added to the antisymmetric contribution. The background could possibly arise from other weak nonresonant photovoltage mechanisms.

The fits agree in an unambiguous manner with the measured results. Hence they can be used to determine the Gilbert damping parameter with high accuracy: $\alpha_G \approx \gamma\Delta H/\omega \approx (0.72\% \pm 0.015\%)$. However, if the magnetization lies parallel or perpendicular to the stripe the photovoltage vanishes [see Eq. (21)]. Hence we can only verify α_G when the magnetization is neither close to being parallel nor perpendicular to our stripe.

The corresponding $\alpha_G=1/\omega\tau$ in the Nickel sample of Egan and Juretschke,[31] can be estimated using the ferromagnetic relaxation time τ from their Table II. It lies in between $\alpha_G=0.12$ and 0.18, so being more than 16 times higher than the value in our sample. This makes the line shape approximation of Sec. II D invalid for their case. Consequently, a

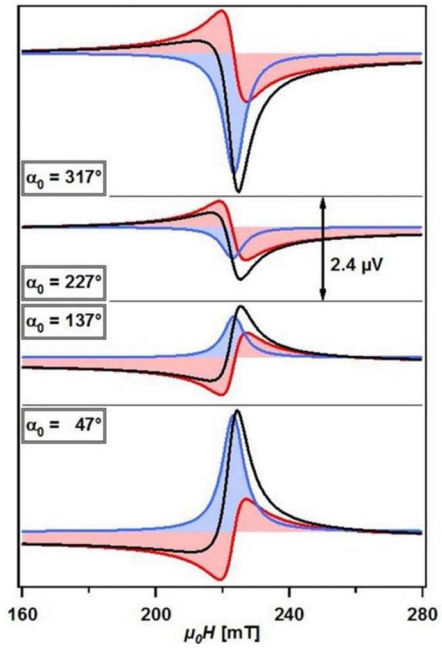

FIG. 9. (Color online) Symmetric and antisymmetric contributions to the asymmetric Lorentz line shape fit from Fig. 8 (black). A small constant background is found and added to the antisymmetric contribution.

much more elaborated line shape analysis[23] appears necessary.

In Fig. 8 the photovoltage along the stripe is presented at four different angles α_0. The signal to noise ratio is about 1000 because of the carefully designed measurement system, where the noise is suppressed to less than 5 nV. Because of this good sensitivity we can verify the matching of our theory from Sec. II with the measurement results in great detail. (See Fig. 10.)

In the following we want to investigate the angular dependence in detail. Therefore, we transform the coordinate system of Eq. (23) according to the transformation presented in

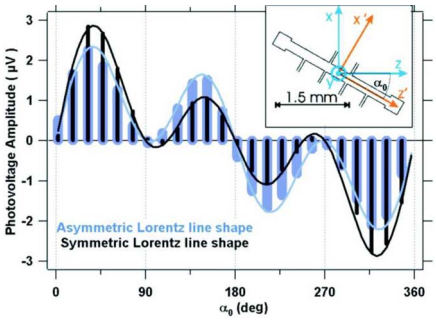

FIG. 10. (Color online) Bars show the angular dependence of the amplitude of the symmetric (U_0^{SYM}, thin bars) and antisymmetric (U_0^{ANT}, thick bars) contribution to the microwave photovoltage at $f=15.0$ GHz. Note that both the symmetric and antisymmetric contribution vanish for $\alpha_0=0°$, 90°, 180°, and 270°. The lines represent the corresponding fits by means of Eq. (34). The inlet shows the geometry of the investigated Permalloy stripe and the coordinate systems from Fig. 3 (note: $\mathbf{z}\|\mathbf{H}$).

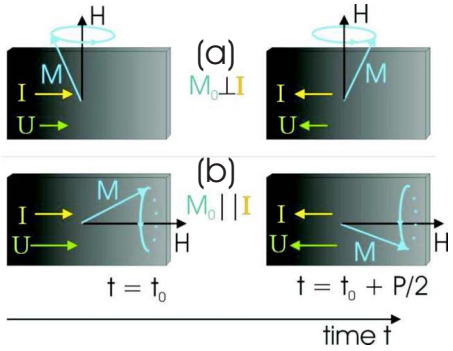

FIG. 11. (Color online) When the magnetic field **H** lies parallel or perpendicular to the stripe, the time average voltage vanishes. (a) **H** lies perpendicular to **I**: Precession of the magnetization **M** leaves (after half a period $P/2$) the angle θ between the axis of **M** and **I** unchanged. Hence the AMR (and so voltage **U**) is also unchanged. The photovoltage vanishes. (b) **H** is parallel to **I**: θ and the AMR stay constant during the precession of **M** and the time average of **I** is zero. This means that only when **H** is neither parallel nor perpendicular to the stripe a photovoltage is generated.

Sec. II A. Doing so we can separate the contributions from $h_{x'}$, h_y, and $h_{z'}$:

$$U_{\mathrm{MW}} = \frac{R_A I_1 \sin(2\alpha_0)}{2M_0}\Big\{[A_{xy}h_y^r + A_{xx}(h_{x'}^i \cos\alpha_0 - h_{z'}^i \sin\alpha_0)]\frac{\Delta H^2}{(H-H_0)^2+\Delta H^2} + [A_{xy}h_y^i + A_{xx}(h_{z'}^r \sin\alpha_0 - h_{x'}^r \cos\alpha_0)]\frac{\Delta H(H-H_0)}{(H-H_0)^2+\Delta H^2}\Big\}. \tag{33}$$

$h_{x'}$, h_y, and $h_{z'}$ are fixed with respect to the hollow brass waveguide and its microwave configuration and do not change when α_0 is varied.

We find that the angular dependence of the line shape in Eq. (33) exhibits two aspects: An overall factor $\sin(2\alpha_0)$ and individual factors ($\sin\alpha_0$, $\cos\alpha_0$, and 1) for the terms belonging to the different spatial components of **h**. The overall factor $\sin(2\alpha_0)$ arises from the AMR photovoltage mechanism and results in vanishing of the photovoltage signal at $\alpha_0=0°$, 90°, 180°, and 270°. This means if $\mathbf{M}_0$ lies either parallel, antiparallel, or perpendicular to the stripe axis. This is illustrated in Fig. 11 and is clearly observed in our measurements (see Fig. 10). We take this as a strong support for the photovoltage being really AMR based.

Another support comes from the similarity with the planar Hall effect.[35] The planar Hall effect generates a voltage U_{PHE} perpendicular to the current in ferromagnetic samples (width W) when the magnetization $\mathbf{M}_0$ lies in the current-voltage plane. It arises as well from AMR and vanishes when $\mathbf{M}_0$ lies either parallel or perpendicular to the current axis.

The similarity arises because of the AMR only generating a transversal resistance when the current is not lying along the principle axis of its resistance matrix (parallel or perpen-

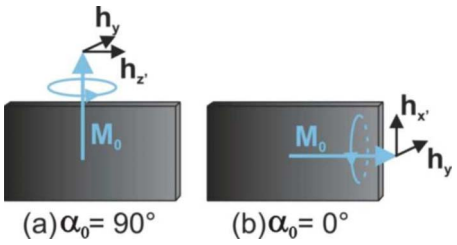

FIG. 12. (Color online) Angular dependent coupling of the magnetization **M** to the dynamic magnetic field $\mathbf{h}=(h_{x'},h_y,h_{z'})$. Only the components of **h** perpendicular to $\mathbf{M}_0$ can excite precession of **M** and therefore generate a dynamic **m**. h_y is always exciting **m**. The excitation strength of $h_{x'}$ and $h_{z'}$ is angular dependent [compare Eq. (33)]. Here the two symmetry cases are shown: **M** (a) perpendicular (only $h_{z'}$ and h_y can excite **M**) and (b) parallel (only $h_{x'}$ and h_y can excite **M**) to the stripe.

dicular to the magnetization). This is the same geometrical restriction as shown above for the microwave photovoltage [see Eq. (21) and Fig. 11].

We want to emphasize the importance that in any of these microwave photovoltage experiments, due to the unusually strong angle dependence, it is important to pay attention to the exact angle adjustment of the sample with respect to the dc magnetic field **H** when measuring under high symmetry conditions (**H** parallel or perpendicular to the stripe) to avoid involuntary signal changes due to small misalignments. As found in 90° out-of-plane configuration[10] already a misalignment as small as a tenth of a degree can yield a tremendous photovoltage change in the vicinity of the FMR.

Finally we want to come back to the individual angular dependencies of the photovoltage contributions arising from the different external magnetic field components. In addition to the $\sin(2\alpha_0)$ proportional dependence of U_{MW} on m_x, also the strength with which m_x is excited by **h** depends on α_0. This is displayed in Fig. 12 and reflected by the three terms in Eq. (33) depending on $h_{x'}$, h_y, and $h_{z'}$ with $\cos\alpha_0$, 1, and $\sin\alpha_0$ factors, respectively. Hence the symmetric U_0^{SYM} and antisymmetric U_0^{ANT} Lorentz line shape contribution to U_{MW} are fitted in Fig. 10 with

$$U_0^{\mathrm{SYM}} = [U_{z'}^S \sin(\alpha_0) + U_{x'}^S \cos(\alpha_0) + U_y^S]\sin(2\alpha_0),$$

$$U_0^{\mathrm{ANT}} = [U_{z'}^A \sin(\alpha_0) + U_{x'}^A \cos(\alpha_0) + U_y^A]\sin(2\alpha_0). \quad (34)$$

From $U_{z'}^S$, $U_{x'}^S$, and U_y^A the dynamic magnetic field components $h_{z'}^i$, $h_{x'}^i$, h_y^i which are 90° out-of-phase with respect to the rf current I_1 can be determined using Eq. (33) and from $U_{z'}^A$, $U_{x'}^A$, and U_y^S we find $h_{z'}^r$, $h_{x'}^r$, and h_y^r which are in phase with I_1.

In principle I_1 can be separately deduced using the bolometric effect[12] as discussed in Sec. IV A. However, for the sample used here our usage of multiple stipes does not allow us to address the bolometric heating to one single stripe. Consequently the strength of I_1 is unknown so that we can not determine **h**, but only $\mathbf{h}I_1$.

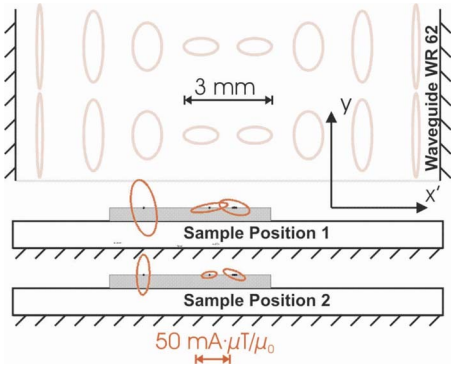

FIG. 13. (Color online) Direction and ellipticity of the rf magnetic field **h** displayed by showing the path $I_1\cdot\mathbf{h}$ passes during one cycle. This is shown at the location of the three stripes (these lie normal to the picture on top of the gray GaAs substrate; the 200 μm wide stripe to the right) for two sample positions. $I_1\cdot\mathbf{h}$ was determined by means of Eq. (33). The upper right path corresponds to the $I_1\cdot\mathbf{h}$ from Table I. The hatched edges indicate metal surfaces reflecting microwaves. Within the waveguide the rf magnetic field **h** corresponding to the TE_{10} mode is displayed in the background.

Besides, considering the special dynamic magnetic field configuration in our rectangular hollow waveguide no rf magnetic field component $h_{z'}$ is expected to be generated along the waveguides narrow dimension (z' axis) by the TE_{01} mode[1] (which is the microwave configuration of our waveguide). It follows that the $\sin(\alpha_0)$ terms in Eq. (34) vanishes. This results in the additional symmetry $U_{\mathrm{MW}}(\alpha_0) = -U_{\mathrm{MW}}(-\alpha_0)$, which is clearly observed in our measurements (see Fig. 10). This symmetry was broken when we used a round waveguide.

The vanishing of $h_{z'}$ in our waveguide will allow us to plot the direction of **h** two-dimensional (instead of three-dimensional) in Fig. 13. A small deviation from the symmetry $U_{\mathrm{MW}}(\alpha_0)=-U_{\mathrm{MW}}(-\alpha_0)$ is however found and arises from a small $h_{z'}$ component (see Table I) which is not displayed in Fig. 13. It might arise from the fact that the rf microwave magnetic field **h** at the waveguide end already deviates from the TE_{01} mode.

TABLE I. Determination of the rf magnetic field **h** at the 200 μm wide stripe at 1 mm distance from the waveguide end by means of Eq. (33). $U_{x',y,z'}^S$, $U_{x',y,z'}^A$: Measured amplitudes of the contributions to the symmetric and antisymmetric Lorentz line shape of U_{MW} [see Eq. (34)] with the angular dependence belonging to x', y, and z', respectively (taken from the fitting in Fig. 10). $A_{xx,xy}$: Corresponding amplitudes of $\chi_{xx,xy}$. $h_{x',y,z'}^r$, $h_{x',y,z'}^i$: rf magnetic field strength calculated from $U_{x',y,z'}^S$, $U_{x',y,z'}^A$ (in-phase and 90° out-of-phase contribution with respect to the current).

	$U_{x',y,z'}^S$	$U_{x',y,z'}^A$	A_{xx}	A_{xy}	$I_1 h_{x',y,z'}^r$	$I_1 h_{x',y,z'}^i$
	(μV)				(mA μT/μ_0)	
x'	+2.60	+2.55	231.1		−15.7	+16.4
y	+0.95	+0.30		97.1	+14.0	+4.4
z'	+0.12	0.00	231.1		0.0	−0.7

D. Determination of the rf magnetic field direction

Using the different angular dependencies of the three symmetric and three antisymmetric terms in Eq. (33) $\mathbf{h}I_1$ can be determined. We make the assumption that the stripe itself does not influence the rf magnetic field configuration, what is at least the case when further reducing its dimensions. Thus the film stripe becomes a kind of detector for the rf magnetic field $\mathbf{h}$.

To test this an array of 36 additional 50 μm wide and 20 μm distant Permalloy stripes of the same height and length as the 200 μm wide stripe described above (see Sec. III A) was patterned beside this one. The 50 μm wide stripes were connected with each other at alternating ends to form a long meandering stripe.[9] Four stripes were elongated on both ends to 300×300 μm^2 Permalloy contact pads. For the outer two stripes and the single 200 μm stripe $\mathbf{h}I_1$ is calculated from the measured photovoltage using Eq. (23). Table I shows the measured voltage and the corresponding $\mathbf{h}I_1$ for the 200 μm stripe at 1 mm distance from the waveguide. $\mathbf{h}I_1$ for all three stripes is displayed in Fig. 13, while positioning the sample at two distances (1 and 3.5 mm, respectively) from the waveguide end. For comparison the rf magnetic field $\mathbf{h}$ configuration of the TE_{01} mode is displayed in the background. From other measurements we can estimate that I_1 lies somewhere in the 1 mA range.

It is worth noting that possible inhomogeneities of the rf magnetic field $\mathbf{h}$ within the Permalloy stripes will be averaged because U_{MW} is linear in $\mathbf{h}$. Determining the sign of the rf magnetic field components from the photovoltage contributions signs exhibits a certain complexity because a lot of attention has to be paid to the chosen time evolution ($e^{i\omega t}$ or $e^{-i\omega t}$) and coordinate system (right hand or left hand). However, the sign only reflects the phase difference with respect to the rf current. The rf current is admittedly not identical for different stripe positions. Consequently the comparison of the rf magnetization phase at different stripe locations is obscured.

It is a specially interesting point concerning microwave photovoltage that the phase of the individual components of the rf magnetic field with respect to the rf current, and therefore also with respect to each other can be determined. The phase information is encoded in the line shape, which is a particular feature of the microwave photovoltage described in this work.

At this point only determining $\mathbf{h}I_1$ is possible because I_1 is unknown. However, in Sec. IV A, an approach to determine I_1 using the bolometric effect is presented. Using this approach the bolometric photoresistance is the perfect supplement for the photovoltage. It delivers unknown I_1 with almost no additional setup.

IV. PHOTORESISTANCE MEASUREMENTS

The principle difficulties when detecting the AMR induced photoresistance are to increase the microwave power for a sufficient signal strength and to reduce the photovoltage signal, which is in general much stronger and superimposes with the photoresistance. We overcome the microwave power problem by using high initial microwave power (316 mW) and a coplanar waveguide (CPW),[10] which emits the microwaves as close as possible to the Permalloy film stripe ($0.137\times20\times2450$ μm^3) with which we detect the photoresistance. Its resistance is found to be $R=880\ \Omega$ and the AMR $R_A=15\ \Omega$. Its magnetic properties (γ, M_0) are almost identical to that of the sample investigated in Sec. III. We use again lock-in technique like in III A with now an additional dc current from a battery to measure resistance instead of voltage. The strong microwave power results in strong rf currents within the sample which give a specially strong photovoltage signal [see Eq. (27)]. To achieve a sufficiently strong photoresistance signal the dc current I_0 and rf current I_1 have to be increased to the maximal value that does not harm the sample (a few mA, hence $I_0\approx I_1$).

Ignoring the trigonometric factors $\sin 2\alpha_0$, $\cos 2\alpha_0$, and $\cos\psi$ as well as the photoresistance term depending on β_1 (that is always smaller than α_1) the photovoltage signal [$U_{MW}=\alpha_1\sin(2\alpha_0)\cos\psi R_A I_1/2$, Eq. (21)] and the photoresistance signal [$\Delta R_{MW}I_0\approx-\alpha_1^2\cos(2\alpha_0)R_A I_0/2$, Eq. (17)] become almost identical. But the major difference is that the photoresistance is multiplied by α_1^2 and the photovoltage only by α_1. As α_1 is particularly small ($<1°$) in our experiments, this means that $\Delta R_{MW}I_0$ is much smaller than U_{MW}. However, suppressing U_{MW} is possible because it vanishes for $\alpha_0=0°$, 90°, 180°, 270° [see Eq. (21)]. A very precise tuning of α_0 with an accuracy below 0.1° is necessary to suppress U_{MW} below $\Delta R_{MW}I_0$. Fortunately in contrast to $|U_{MW}|$, $|\Delta R_{MW}|$ is maximal for $\alpha_0=0°$, 90°, 180°, 270°. In the following, we will first discuss the bolometric photoresistance arising from microwave heating of the sample and afterwards the AMR induced photoresistance that is discussed above.

A. Bolometric (nonresonant)

The AMR-induced ΔR_{MW} is not the only photoresistive effect present in our Permalloy film stripe. Also nonresonant heating by the microwave rf current I_1 results in a (bolometric) photoresistance. The major difference compared to the AMR-based photoresistance is that the bolometric photoresistance is almost independent of the applied dc magnetic field H and that its reaction time to microwave exposure is much longer (in the order of ms) than that of the AMR-based photoresistance ($1/\alpha_G\omega$, in the order of ns).[12] The nonresonant bolometric photoresistance is found with a typical strength of $(\Delta R/R)/P=0.2$ ppm/mW (see Fig. 14).

The bolometric heating power P_{bol} arises from resistive dissipation of the rf current I_1 in the sample ($P_{bol}=\langle RI^2\rangle=RI_0^2+RI_1^2/2$). This can hence be used to determine I_1, which is otherwise an unknown in Eq. (27). I_1 can be determined for example by finding the corresponding dc current I_0 with the same bolometric resistance change. However, especially in the sample we use the thermal conductivity of the GaAs crystal on which our Permalloy stripes were deposited is so high (55 W/m K) that the different stripes are strongly thermally coupled. Thus we cannot address the bolometric signal of one stripe solely to the rf current of the same stripe. This effect was verified comparing the resistance changes from one stripe while applying a dc current through an other stripe. Hence determination of $|I_1|$ by means of Eq. (27) is

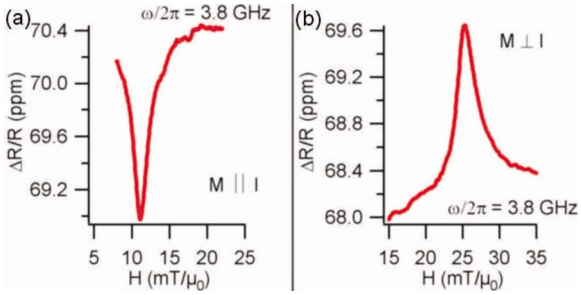

FIG. 14. (Color online) Photoresistance ΔR_{MW} measurement (stripe resistance R). The curves show the difference between the signals ΔU with $I_0=+5$ mA and $I_0=-5$ mA at $P=316$ mW: $\Delta R=[\Delta U(I_0=+5\ \mathrm{mA})-\Delta U(I_0=-5\ \mathrm{mA})]/10$ mA. The subtraction suppresses the photovoltage dependence on absolute $|I_0|$ (for example from bolometric AMR change). For both curves the dc magnetic field **H** (and so **M**) was applied within the film plane, but for (a) parallel to the stripe (and hence to the dc current I_0) and for (b) perpendicular. A nonresonant background of about 70 ppm from bolometric photoresistance is found. It is decreases by about 1.2 ppm when the sample is turned from parallel to perpendicular configuration. This is caused by the 1.7% AMR which changes R and the bolometric signal proportionally. The FMR signal has almost Lorentz line shape and its position is significantly changing when the sample is turned from parallel to perpendicular position (see Sec. IV B).

only possible when using a substrate material with low heat conductance (e.g., glass) or by not depositing more than one stripe.

B. AMR based (resonant)

In contrast to the nonresonant bolometric photoresistance in Sec. IV A, the typically 50 times weaker resonant AMR-based photoresistance is very hard to detect. After visualizing it by using the CPW and turning the sample into a high symmetry position (parallel or perpendicular to **H**) it is still necessary to regard the difference of the photoresistance measured with the same current strength but with reversed current sign instead of measuring with only one current direction. This eliminates the remaining still significant photovoltage signal, which depends on the absolute current strength possibly due to bolometric AMR change.

Measurement results are presented in Fig. 14 for $f=3.8$ GHz. There it can be seen that (as deduced in Sec. II C), if the stripe lies parallel to the magnetization, the AMR is maximal and the resistance decreases when the FMR is excited (negative photoresistance). In contrast in the perpendicular case the AMR is minimal and we measure a resistance increase (positive photoresistance). This behavior is schematically explained in Fig. 15. The curves in Fig. 14 show the photoresistance at the FMR with symmetric Lorentz line shape as predicted in Sec. II C.

Using Eq. (9) we calculate $\mu_0 H_0=16.6$ mT. However, a deviation of H_0 is found in both, parallel ($\mu_0 H_0=11.1$ mT) and perpendicular ($\mu_0 H_0=25.3$ mT), configuration. This is due to demagnetization which gives rise to an FMR shift with respect to the result from the infinite film approximation [compare Eq. (31)]. $N_x=0.7\%$ can be assumed because of this shift.

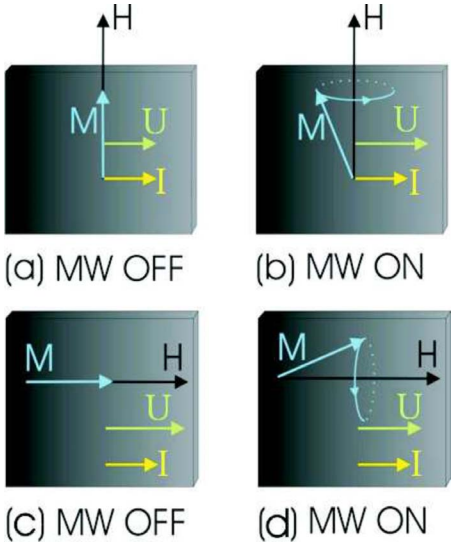

FIG. 15. (Color online) Demonstration of the angular dependence of the microwave photovoltage: Without microwaves [(a), (c)] the AMR is (a) minimal in perpendicular configuration of **M** and **I** and (c) maximal in parallel configuration. When the microwaves are switched on the resistance (b) increases in parallel configuration and (d) decreases in perpendicular configuration.

Using Eq. (16) we find that for our conditions $m_x/m_y=7.9i$. Consequently, we can neglect the contribution from $\beta_1=|m_y|/M_0$ in Eq. (17) and find $|m_x|=13$ mT using $\Delta R_{\mathrm{MW}}=(\Delta R/R)R=1.23$ mΩ (from Fig. 14) and thus $\alpha_1=\sqrt{2\Delta R_{\mathrm{MW}}/R_A}=0.73°$ and $\beta_1=\alpha_1/|m_x/m_y|=0.09°$. The smallness of β_1 is the reason for the resonant photoresistance strength being almost identical for $\mathbf{M}\|\mathbf{I}$ and $\mathbf{M}\perp\mathbf{I}$ (although the sign is reversed). We must expect $|m_x|$, α_1, and β_1 to be even a little bit larger due to our lock-in measurement technique only detecting the sinusoidal contribution to the square wave signal from the microwaves.

The photoresistive decrease is in accordance with that found by Costache *et al.*[13] There the magnetization is aligned with the current ($\alpha_0=0$). Thus applying an rf magnetic field decreases the AMR from R_A to $R_A\cos^2\theta_c$. This is used to determine the precession cone angle θ_c by assuming $\theta_c=\alpha_1=\beta_1$.

The height to width ratio of the strip is 35 nm to 300 nm. Because of the magnetization lying along the stripe,[13] the magnetization precession strongly deviates from being circular. Using the corresponding parameters $\mu_0 M_0=1.06$ T, $\gamma=2\pi\mu_0\times 28$ GHz/T, and $\omega/2\pi=10.5$ GHz), we find from Eq. (16) that the ratio of the amplitudes is $m_x/m_y=3.15i$. This indicates strongly elliptical precession and suggests that distinguishing α_1 and β_1 would provide a refined description compared to that using the cone angle θ_c, as discussed in Sec. II C.

V. CONCLUSIONS

We have presented a comprehensive study of dc electric effects induced by ferromagnetic resonance in Py microstrips. A theoretical model based on a phenomenological approach to magnetoresistance is developed and compared with

experiments. These provide a consistent description of both photovoltage and photoresistance effects.

We demonstrate that the microwave photoresistance is proportional to the square of magnetization precession amplitude. In the special case of circular magnetization precession, the photoresistance measures its cone angle. In the general case of arbitrary sample geometry and elliptical precession, we refine the cone angle concept by defining two different angles, which provide a precise description of the microwave photoresistance (and photovoltage) induced by elliptical magnetization precession. We show that the microwave photoresistance can be either positive or negative, depending on the direction of the dc magnetic field.

In contrast to the microwave photoresistance, we find that the microwave photovoltage is proportional to the product of the in-plane magnetization precession component with the rf current. Consequently, it is sensitive to the magnetic field dependent phase difference between the rf current and the rf magnetization. This results in a characteristic asymmetric photovoltage line shape, which crosses zero when the rf current and the in-plane component of the rf magnetization are exactly 90° out of phase. Therefore, the microwave photovoltage provides a powerful insight into the phase of magnetization precession, which is usually difficult to obtain.

We demonstrate that the asymmetric photovoltage line shape is strongly dependent on the dc magnetic field direction, which can be explained by the directional dependence of the magnetization precession excitation. By using the model developed in this work, and by combining such a sensitive geometrical dependence of the microwave photovoltage with the bolometric photoresistance which independently measures the rf current, we are now in a position to detect and determine the external rf magnetic field vector, which is of long standing interest with significant potential applications.

ACKNOWLEDGMENTS

We thank G. Roy, X. Zhou, and G. Mollard for technical assistance and D. Heitmann, U. Merkt, and the DFG for the loan of equipment. N.M. is supported by the DAAD. This work has been funded by NSERC and URGP grants to C.-M.H.

*nmecking@physnet.uni-hamburg.de
†hu@physics.umanitoba.ca

[1] B. S. Guru and H. R. Hiziroglu, *Electromagnetic Field Theory Fundamentals*, 2nd ed. (Cambridge University Press, Cambridge, UK, 2004).
[2] B. A. Gurney *et al.*, in *Ultrathin Magnetic Structures IV*, edited by B. Heinrich and J. A. C. Bland (Springer, Berlin, 2004), Chaps. 6, 7 and 8.
[3] J.-G. Zhu, and Y. Zheng, in *Spin Dynamics in Confined Magnetic Structures I*, edited by B. Hillebrands and K. Ounadjela (Springer, Berlin, 2002), pp. 289–323.
[4] A. A. Tulapurkar *et al.*, Nature (London) **438**, 339 (2005).
[5] J. C. Sankey, P. M. Braganca, A. G. F. Garcia, I. N. Krivorotov, R. A. Buhrman, and D. C. Ralph, Phys. Rev. Lett. **96**, 227601 (2006).
[6] A. Azevedo, L. H. Vilela Leo, R. L. Rodriguez-Suarez, A. B. Oliveira, and S. M. Rezende, J. Appl. Phys. **97**, 10C715 (2005).
[7] E. Saitoh, M. Ueda, H. Miyajima, and G. Tatara, Appl. Phys. Lett. **88**, 182509 (2006).
[8] M. V. Costache, M. Sladkov, S. M. Watts, C. H. van der Wal, and B. J. van Wees, Phys. Rev. Lett. **97**, 216603 (2006); J. Grollier, M. V. Costache, C. H. van der Wal, and B. J. van Wees, J. Appl. Phys. **100**, 024316 (2006).
[9] Y. S. Gui, S. Holland, N. Mecking, and C.-M. Hu, Phys. Rev. Lett. **95**, 056807 (2005).
[10] Y. S. Gui, N. Mecking, X. Zhou, Gwyn Williams, and C.-M. Hu, Phys. Rev. Lett. **98**, 107602 (2007).
[11] Y. S. Gui, N. Mecking, and C.-M. Hu, Phys. Rev. Lett. **98**, 217603 (2007).
[12] Y. S. Gui, N. Mecking, A. Wirthmann, L. H. Bai, and C.-M. Hu, Appl. Phys. Lett. **91**, 082503 (2007).
[13] M. V. Costache, S. M. Watts, M. Sladkov, C. H. van der Wal, and B. J. van Wees, Appl. Phys. Lett. **89**, 232115 (2006).
[14] A. Yamaguchi, H. Miyajima, T. Ono, Y. Suzuki, S. Yuasa, A. Tulapurkar, and Y. Nakatani, Appl. Phys. Lett. **90**, 182507 (2007); A. Yamaguchi, H. Miyajima, T. Ono, Y. Suzuki, S. Yuasa, A. Tulapurkar, and Y. Nakatani, *ibid.* **90**, 212505 (2007).
[15] Dong Keun Oh *et al.*, J. Magn. Magn. Mater. **293**, 880 (2005); Je-Hyoung Lee and Kungwon Rhie, IEEE Trans. Magn. **35**, 3784 (1999).
[16] S. T. Goennenwein, S. W. Schink, A. Brandlmaier, A. Boger, M. Opel, R. Gross, R. S. Keizer, T. M. Klapwijk, A. Gupta, H. Huebl, C. Bihler, and M. S. Brandt, Appl. Phys. Lett. **90**, 162507 (2007).
[17] J. C. Slonczewski, J. Magn. Magn. Mater. **159**, L1 (1996).
[18] L. Berger, Phys. Rev. B **54**, 9353 (1996).
[19] L. Berger, Phys. Rev. B **59**, 11465 (1999).
[20] A. Brataas, Yaroslav Tserkovnyak, Gerrit E. W. Bauer, and Bertrand I. Halperin, Phys. Rev. B **66**, 060404(R) (2002).
[21] Xuhui Wang, Gerrit E. W. Bauer, Bart J. van Wees, Arne Brataas, and Yaroslav Tserkovnyak, Phys. Rev. Lett. **97**, 216602 (2006).
[22] C.-M. Hu, C. Zehnder, Ch. Heyn, and D. Heitmann, Phys. Rev. B **67**, 201302(R) (2003).
[23] H. J. Juretschke, J. Appl. Phys. **31**, 1401 (1960).
[24] R. H. Silsbee, A. Janossy, and P. Monod, Phys. Rev. B **19**, 4382 (1979).
[25] W. M. Moller and H. J. Juretschke, Phys. Rev. B **2**, 2651 (1970).
[26] D. Polder, Philos. Mag. **40**, 99 (1949).
[27] T. L. Gilbert, IEEE Trans. Magn. **40**, 3443 (2004).
[28] L. Landau and L. Liftshitz, Phys. Z. Sowjetunion **8**, 153 (1935).
[29] R. E. Camley and D. L. Mills, J. Appl. Phys. **82**, 3058 (1997).
[30] C. Kittel, Phys. Rev. **73**, 155 (1948).
[31] W. G. Egan and H. J. Juretschke, J. Appl. Phys. **34**, 1477 (1963).
[32] J. N. Kupferschmidt, Shaffique Adam, and P. W. Brouwer, Phys. Rev. B **74**, 134416 (2006).
[33] S. I. Kiselev, J. C. Sankey, I. N. Krivorotov, N. C. Emley, R. J. Schoelkopf, R. A. Buhrman, and D. C. Ralph, Nature (London) **425**, 380 (2003).
[34] M. S. Sodha and N. C. Srivasta, *Microwave Propagation in Ferrimagnets* (Plenum Press, New York, 1981).
[35] K. L. Yau and J. T. H. Chang, J. Phys. F: Met. Phys. **1**, 38 (1971).